Journal of Pharmacy

ORIGINAL ARTICLE Open Access

Antibacterial Potential of *Ximenia americana* L. Olacaceae: Molecular Docking, Molecular Dynamics, and ADMET Prediction

Mubarak Muhammad Dahiru[1*], Abdulazeez Mumsiri Abaka[2] and Ibrahim Ya'u[2]

ABSTRACT

Introduction: The devastating effect of persistent and recurrent bacterial infections coupled with antibiotic resistance is a driving force for prospects into alternative antibacterial therapeutics to achieve treatment. This study investigates the antibacterial potential of *Ximenia americana* (XA) *via* molecular docking, molecular dynamics, and ADMET approach.

Materials and methods: The ligands and target were downloaded from respective databases and docked using PyRx software followed by molecular dynamics simulation (MDS) with iMOD and CABflex 2.0 online servers then ADMET, drug likeness, lead likeness, and medicinal chemistry predictions of the top docked ligands using pkCSM and SwissADME online servers.

Results: Stigmasterol exhibited the lowest binding affinity and inhibition constant respectively with all the targets; enoyl-acyl-carrier-protein reductase (-7.1 kcal/mol and 6.16 µM), Penicillin-binding Protein 2X (-8.8 kcal/mol and 0.35 µM), dihydrofolate reductase (-9.6 kcal/mol and 0.09 µM), dihydropteroate Synthase (-7.8 kcal/mol and 1.89 µM), UDP-N-acetylglucosamine enolpyruvyl transferase (-7.1 kcal/mol and 6.16 µM), and topoisomerase IV (-7.8 kcal/mol and 1.89 µM). The MDS showed several cluster displacements and residue fluctuations with the docked targets with higher residue fluctuations observed for enoyl-acyl-carrier-protein reductase (11.33 Å), Penicillin-binding Protein 2X (4.67 Å), dihydrofolate reductase (3.61 Å), dihydropteroate Synthase (4.97 Å), UDP-N-acetylglucosamine enolpyruvyl transferase (3.38 Å), and topoisomerase IV (4.35 Å). 4,4-Dimethylcyclohex-2-en-1-ol exhibited superior overall ADMET properties, oral bioavailability, drug-likeness, and medicinal chemistry.

Conclusion: Conclusively, Stigmasterol and 4,4-Dimethylcyclohex-2-en-1-ol might be responsible for the antibacterial effect of XA. Although the latter showed better interaction with the target proteins, the former showed better ADMET properties, oral bioavailability, drug-likeness, and medicinal properties. However, improvement in these properties might enhance their antibacterial activity.

ARTICLE HISTORY:

Received: 30 September 2023
Accept: 11 December 2023
Published: 31 January 2024

KEYWORDS:

ADMET, Molecular docking, Molecular dynamics, Stigmasterol, *Ximenia americana*

HOW TO CITE THIS ARTICLE:

Dahiru, M. M., Abaka, A. M. and Ya'u, I. (2023). Antibacterial Potential of *Ximenia americana* L. Olacaceae: Molecular Docking, Molecular Dynamics, and ADMET Prediction. *Journal of Pharmacy,* 4(1), 51-67.

doi: 10.31436/jop.v4i1.252

***Corresponding author:**
Mubarak Muhammad Dahiru
Email: mubaraq93@adamawapoly.edu.ng

Authors' Affiliation:

[1]*Department of Pharmaceutical Technology, Adamawa State Polytechnic, Yola, 640101 Adamawa State, Nigeria*
[2] *Department of Science Laboratory Technology, Adamawa State Polytechnic, Yola, 640101 Adamawa State, Nigeria*

JOP

Introduction

Bacterial infections are regarded as a major culprit leading to mortality worldwide which is further complicated by the emergence of antimicrobial resistance (AR) (Uddin et al., 2021). Antibiotic abuse in clinical practice contributes to the enhanced evolution of microbes *via* mutation into more infectious and antibiotic-resistant strains, thus creating a major problem in treatment and threatening global health (Kapoor et al., 2017). In bacteria, AR emerges as a result of antibiotic inactivation, metabolic pathways bypass, modified target, and permeability (Kapoor et al., 2017). This mechanism forms a basis for survival and enhances their endurance to antibiotic effects previously lethal to their survival (Zaman et al., 2017). Additionally, biofilm formation has also facilitated AR, further complicating treatment (Uddin et al., 2021). Although the use of antibiotics is acceptable worldwide, bacteria evolution into antibiotic resistance strains is a global concern due to the re-emergence of drug-resistant infections (Gajdács & Albericio, 2019). Antibiotics target DNA replication proteins, cell walls, and macromolecule synthesis, which are processes needed for bacterial survival (Kapoor et al., 2017). However, the instinct for survival and adaptation to adverse conditions associated with bacteria drives evolutionary mechanisms including genetic modifications that lead to AR (MacGowan & Macnaughton, 2017).

Although multiple drugs or combined therapies are applied in the treatment of bacterial infections, the problem of multidrug resistance further emerges (Uddin et al., 2021), thus the prospects for alternatives such as plant-based sources. Plant-based drugs include phytochemicals produced in plants against predators and climate change to ensure their survival (Doughari, 2012). Some of these phytochemicals are lethal to bacteria targeting multiple processes and pathways simultaneously and synergistically (Dahiru et al., 2023b). Thus, might be regarded as an alternative to conventional drugs in combating AR. The use of plants in the management of bacterial ailments garnered attention due to their affordability, safety, and acceptability. Thus, various plants of varying efficacy are used for antibiotic purposes to achieve therapeutic goals (Chassagne et al., 2021). Moreover, previous studies reported the antibacterial activity of different plant extracts revealing the bactericidal and inhibitory effects of the plant extracts (Dahiru et al., 2023a; Dahiru et al., 2023b; Ebbo et al., 2019). *X. americana* has been associated with different antibacterial effects (Agustina & Nugroho, 2021; Kiessoun et al., 2018; Maikai et al., 2009) including inhibiting biofilm formation (Bakrim et al., 2022), and antibiotic synergistic effect (de Menezes et al., 2019). In traditional medicine, the plant is used for urinary tract infections, diarrhea, anti-parasitic, leprotic ulcers, antiseptic, and skin infections (Monte et al., 2012).

Different computational techniques are employed in drug discovery and design to predict the possible mechanism of action of compounds including molecular docking, molecular dynamics, and the ADMET (absorption, distribution, metabolism, excretion, and toxicity) approach (Clegg & Mac Gabhann, 2015; Lin et al., 2020; Sliwoski et al., 2014). In the molecular docking approach, ligands (compounds) and targets (proteins) are downloaded from various databases and prepared by energy minimization, water molecules, and heteroatom removal for docking (Raval & Ganatra, 2022). The ligand is docked into the binding pocket of the target to calculate the binding affinity or energy and the interactions (Raval & Ganatra, 2022). This can be further subjected to molecular dynamics simulation to predict the possible residue motion with the structure of the target (Hollingsworth & Dror, 2018). Previous studies revealed many compounds with various antimicrobial properties present in X. *americana* (Dahiru et al., 2022). However, the exact mechanisms of action of the compounds are yet to be identified. In this study, the antibacterial activity of the compounds previously identified in *X. americana* was investigated *in silico via* molecular docking and molecular dynamics to determine its major antibacterial compounds followed by ADMET predictions of the compounds for drug- and lead-likeness potential.

Materials and methods

Materials

Hardware Specification

A personal computer was used for the present study with 8 GB RAM with an AMD 2.1 GHz to 2.9 GHz Elite Quad-core A10-5745M accelerated processer and AMD Radeon HD 8610G graphics with up to 3053 MB total graphics memory.

Ligands and Targets

The ligands (compounds) previously identified in our study (Dahiru et al., 2022) and targets used in our study were downloaded from the PubChem (https://pubchem.ncbi.nlm.nih.gov) and RSCB (https://www.rcsb.org) databases in SDF and PDB formats respectively. The ligands were energy-minimized using the PyRx – Python Prescription software (version 0.8) while water molecules, heteroatoms, attached ligands, and extra chains were removed from the targets using AutoDockTools (version 1.5.7) (Sanner, 1999) before docking. The list of ligands is presented in Table 1 including their PubChem ID.

Table 1: List of Ligands

Name	PubChem ID
Catechol	289
Phloroglucinol	359
Hydroquinone	785
Palmitic Acid	985
Pyrogallol	1057
Methyl palmitate	8181
5-Methyl-1H-pyrazole-3-carboxylic acid	9822
Hydroxyquinol	10787
Tridecane	12388
Pentadecanoic acid	13849
2-Isopropoxyphenol	20949
2-dodecoxyethanol	24750
5-Acetoxymethyl-2-furaldehyde	66349
6-Methylpyridazin-3(2H)-one	83346
3,4-dimethylcyclohexanol	97960
2,6-Heptanedione	100532
5-Butylnonane	300476
Oleic Acid	445639
3,8-Dimethyldecane	519396
Tetradec-13-enal	522841
Stigmasterol	5280794
1-(1-Butenyl) pyrrolidine	5357122
7,11-Hexadecadien-1-ol, acetate, (7Z,11Z)-	5363265
9-Tetradecenal, (Z)-	5364471
4,4-Dimethylcyclohex-2-en-1-ol	19771306

The docking targets are presented in Table 2 depicting their RSCB PDB ID and the docking grid box center.

Table 2: List of Targets

Name	PBD ID	Grid box center		
		X	Y	Z
Enoyl-acyl-carrier-protein Reductase (FabI)	1LX6	-2.28	22.61	134.79
Penicillin-binding protein 2X (PBP2X)	5OJ0	33.51	-16.54	54.36
Dihydrofolate reductase (DHFR)	1RG7	-1.21	21.34	21.20
Dihydropteroate synthase (DHPS)	5V79	-18.37	7.09	103.33
UDP-N-acetylglucosamine enolpyruvyl transferase (MurA)	2RL2	28.79	-53.59	45.05
Topoisomerase IV (TopoIV)	3FV5	12.93	-0.80	2.39

Methods

Molecular Docking (MD) and Molecular Dynamics Simulation (MDS)

The docking pockets were initially identified using the Prankweb online server (https://prankweb.cz) (Jendele et al., 2019) to determine the docking coordinates. The docking protocol was carried out using the PyRx software *via* the Vina wizard to determine the binding affinity (BA) with exhaustiveness set to 16. The inhibition constant (Ki) was evaluated from the BA using the equation Ki = exp ΔG/RT where T=298.15 K (temperature) and R=1.985 x 10^{-3} $kcal^{-1}$ mol^{-1} k^{-1} (the universal gas constant) and ΔG = binding affinity (Ortiz et al., 2019). Furthermore, the ligand-target docked complexes were saved in PDB and visualized in 2D and 3D using Biovia Discovery Studio Visualizer (version 16.1.0). Additionally, only the top three compounds with the least BA and Ki were selected and presented. Lastly, the top docked complex with the least BA and Ki was subjected to MDS using the iMODs server (https://imods.iqfr.csic.es) (iMODS) (López-Blanco et al., 2014) and CABs-flex v2.0 (http://biocomp.chem.uw.edu.pl/CABSflex2/index) (Kurcinski et al., 2019) online servers to identify cluster and residue displacements denoted by the root-mean-square fluctuation (RMSF) respectively.

ADMET Prediction

The ADMET of the compound with the least BA and Ki interaction was further predicted using the pkCSM online server (https://biosig.lab.uq.edu.au/pkcsm) (Pires et al., 2015) and the SwissADME server (http://www.swissadme.ch) (Daina et al., 2017) for its drug-likeness and medicinal chemistry.

Results

The BA and Ki of the compounds docked with FabI and PBP2X are displayed in Table 3. Stigmasterol exhibited superior binding interaction with FabI demonstrating the least BA (-7.1 kcal/mol) and Ki (6.16 µM) followed by 4,4-Dimethylcyclohex-2-en-1-ol with -5.5 kcal/mol and 92 µM next to 7,11-Hexadecadien-1-ol, acetate, (7Z,11Z) with -5.0 kcal/mol and 214.24 µM. The docking interactions with PBP2X revealed stigmasterol as the most favorable among the compounds with BA and Ki of -8.8 kcal/mol and 0.35 µM respectively next to 4,4-Dimethylcyclohex-2-en-1-ol with -7 kcal/mol and 7.30 µM, while the least favorable was 7,11-Hexadecadien-1-ol, acetate, (7Z,11Z) with -5.3 kcal/mol and 129.05 µM, a similar pattern observed in that of FabI.

The binding interactions of FabI with stigmasterol are presented in Figure 1 showing the 2D and 3D dock pose and depicting the hydrogen bonds and alkyl interactions. Single conventional hydrogen was observed with LYS163 while six alkyl interactions were also observed.

Table 3: Binding affinity and Ki of the interaction of FabI and PBP2X with the compounds

Target	Ligand	Binding Affinity (kcal/mol)	Ki (µM)
FabI	Stigmasterol	-7.1	6.16
	4,4-Dimethylcyclohex-2-en-1-ol	-5.5	92.04
	7,11-Hexadecadien-1-ol, acetate, (7Z,11Z)	-5.0	214.24
PBP2X	Stigmasterol	-8.8	0.35
	4,4-Dimethylcyclohex-2-en-1-ol	-7.0	7.30
	7,11-Hexadecadien-1-ol, acetate, (7Z,11Z)	-5.3	129.05

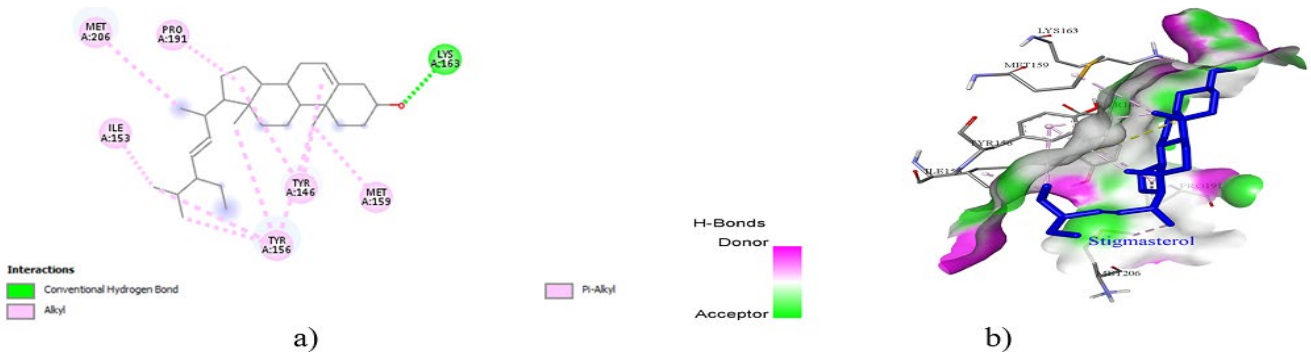

Figure 1: Binding interactions and docked pose of stigmasterol with FabI; a) 2D and b) 3D

The residue fluctuation and cluster displacement of FabI and stigmasterol-FabI docked complex are shown in Figure 2. Increased residue fluctuations were observed at GLY2 (11.33 Å), SER16 (2.12 Å), ASN41 (2.50 Å), CYS210 (1.14 Å), and ASN257 (3.52 Å) though there was a decrease at ASP103 (2.51 Å) compared to the apoenzyme. Although the highest cluster movement was observed at the N-terminal end of the peptide, a lesser displacement was also observed close to the midchain.

.

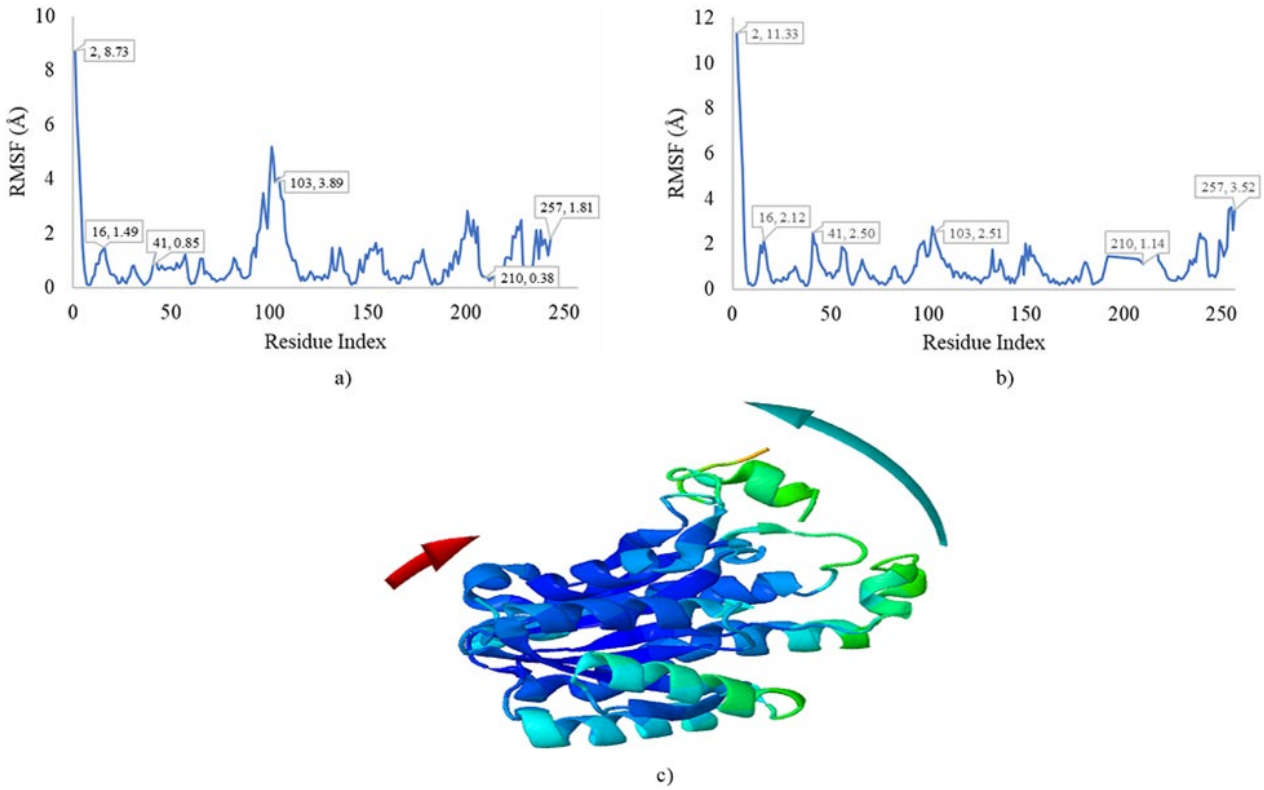

Figure 2: MDS result depicting residue fluctuation of; a) FabI, b) Stigmasterol-FabI docked complex, and c) Cluster displacement of the docked complex (blue and red arrows indicate higher and lower displacements respectively)

The binding interactions of PBP2X with the stigmasterol are presented in Figure 3 highlighting the residue involved in 2D and 2D dock pose. A π-alkyl interaction with PHE450 was observed in addition to a π-sigma with TRP374.

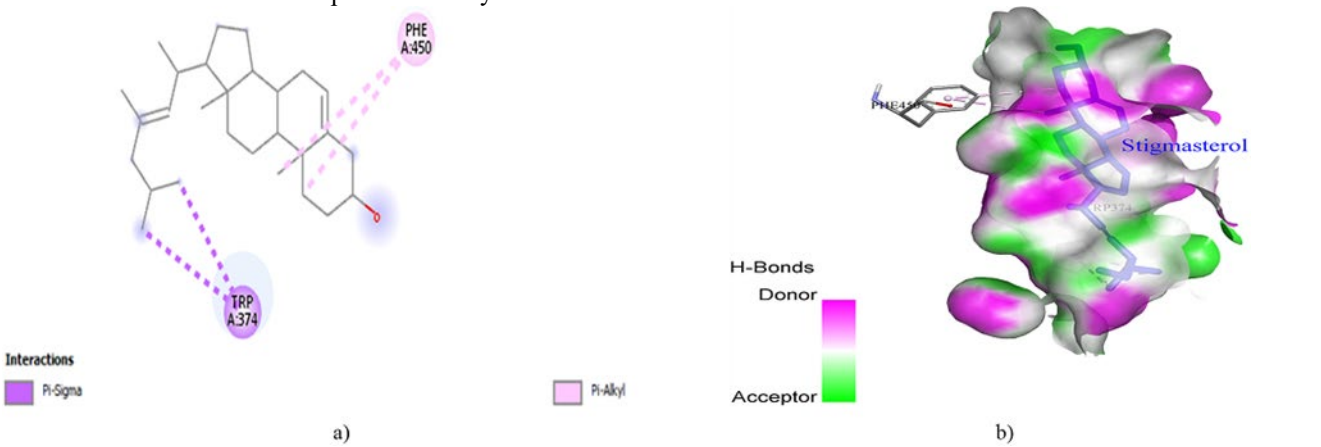

Figure 3: Binding interactions and docked pose of stigmasterol with PBP2X; a) 2D and b) 3D

Figure 4 presents the MDS results for PBP2X and stigmasterol-PBP2X docked complex showing the fluctuating residues and cluster movement. Several increased residue displacements were observed with the highest by ILE318 (4.67 Å) while others include PRO144 (3.31 Å), GLN629 (4.54 Å), GLY677 (3.13 Å), and ASP750 (4.24 Å). However, a notable decrease in ASP555 (2.07 Å) and ASN580 (3.09 Å) was also observed. Additionally, cluster displacements were seen at both terminal clusters of the peptide and within its structure though the highest was at the N-terminal.

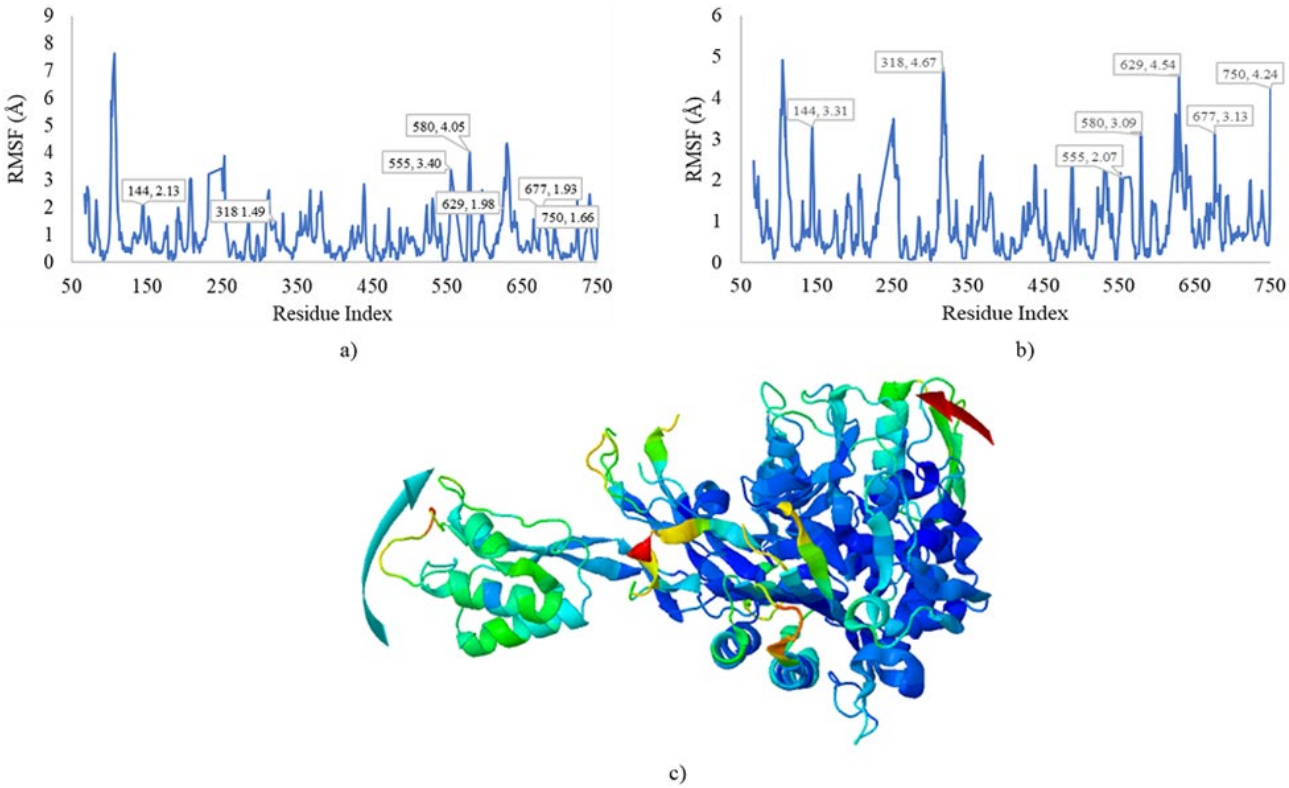

Figure 4: MDS result depicting residue fluctuation of; a) PBP2X, b) Stigmasterol-PBP2X docked complex, and c) Cluster displacement of the docked complex (blue and red arrows indicate higher and lower displacements respectively)

Table 4 displays the BA and Ki of the binding affinity and Ki of DHFR and DHPS with the compounds. Stigmasterol exhibited a superior and more favorable interaction with DHFR with BA and Ki of -9.6 kcal/mol and 0.09 µM respectively followed by 4,4-dimethylcyclohex-2-en-1-ol with -7.7 kcal/mol and 2.24 µM. Oleic acid exhibited the highest BA (-6.5 kcal/mol) and Ki (17 µM) when docked with DHFR. Furthermore, stigmasterol showed the BA (-7.8 kcal/mol) and Ki (1.89 µM) when docked with DHPS. These values are more favorable interactions compared to the other compounds. Specifically, 4,4-dimethylcyclohex-2-en-1-ol showed a BA of -5.7 kcal/mol and Ki of 65.65 µM, while 5-acetoxymethyl-2-furaldehyde demonstrated the least favorable values with -5.3 kcal/mol and 129.05 µM, respectively.

The 2D and 3D dock poses depicting the binding interactions of the stigmasterol-DHFR docked complex are presented in Figure 5. A total of seven alkyl interactions were observed with ILE50, LEU28, LEU54, PHE31, ILE94, ALA19, and LYS32.

Table 4: Binding affinity and Ki of the interaction of DHFR and DHPS with the compounds

Target	Ligand	Binding Affinity (kcal/mol)	Ki (µm)
DHFR	Stigmasterol	-9.6	0.09
	4,4-Dimethylcyclohex-2-en-1-ol	-7.7	2.24
	Oleic Acid	-6.5	16.99
DHPS	Stigmasterol	-7.8	1.89
	4,4-Dimethylcyclohex-2-en-1-ol	-5.7	65.65
	5-Acetoxymethyl-2-furaldehyde	-5.3	129.05

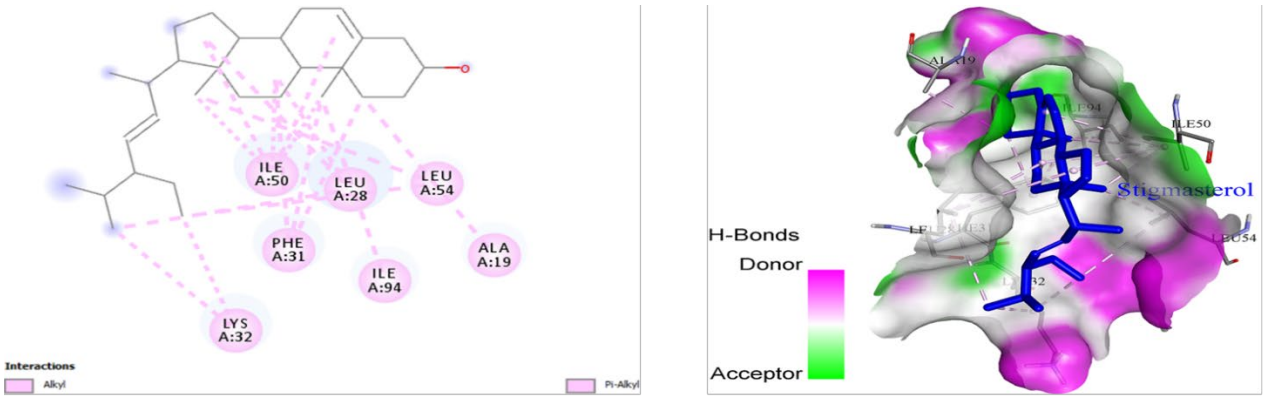

a) b)

Figure 5: Dock poses and interactions of stigmasterol with DHFR; a) 2D and b) 3D

Figure 6 displays the MDS result of DHFR and stigmasterol-DHFR complex revealing the residue fluctuation and cluster movement. All the residues were displaced with the highest (3.61 Å) displacement observed around the midchain (GLY67) of the peptide with cluster movement at both terminals. Additionally, notably increased displacements by PRO21 (2.70 Å) and a decrease by GLY56 (1.91 Å) were observed. Cluster displacements were observed within the peptide chain with the highest around the N-terminal to midchain of the peptide.

The binding interactions of stigmasterol with DHPS are shown in Figure 7 revealing the docked pose in 2D and 3D. Exactly five alkyl interactions were observed with ARG63, HIS257, ILE20, PHE190, and LYS221 stabilizing the docked complex.

Figure 8 depicts the cluster displacement and residue fluctuation of DHPS and stigmasterol-DHPS docked complex MDS. The highest (4.97 Å) residue displacement was seen at the midchain (THR147) of the peptide though there were increased displacements by MET1 (2.19 Å), HIS14 (2.48 Å), and ASN35 (3.33 Å) with decrease by PRO80 (0.22 Å), ALA111 (0.56 Å), LEU134 (0.38 Å), ALA170 (0.38 Å), and LYS221 (1.78 Å). The C-terminal demonstrated the highest cluster displacement though both terminals were displaced including the lower displacement at the midchain of the peptide.

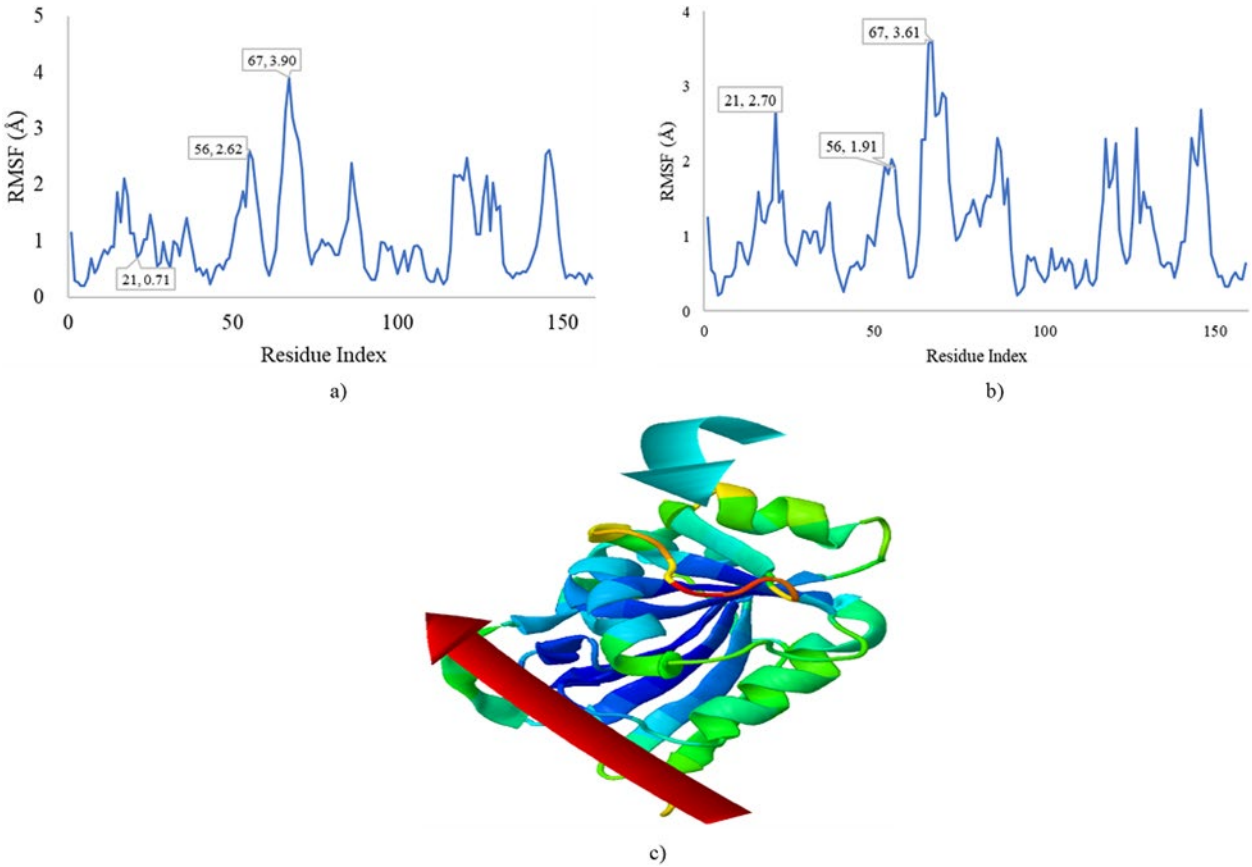

Figure 6: MDS result depicting residue fluctuation of; a) DHFR, b) Stigmasterol-DHFR docked complex, and c) Cluster displacement of the docked complex (blue and red arrows indicate higher and lower displacements respectively)

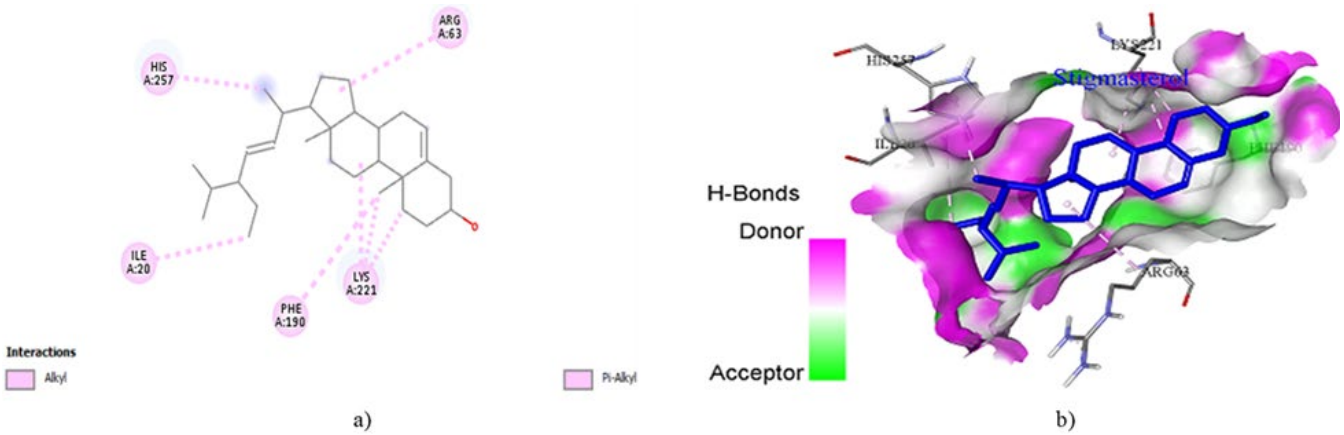

Figure 7: Dock poses and interactions of stigmasterol with DHPS; a) 2D and b) 3D

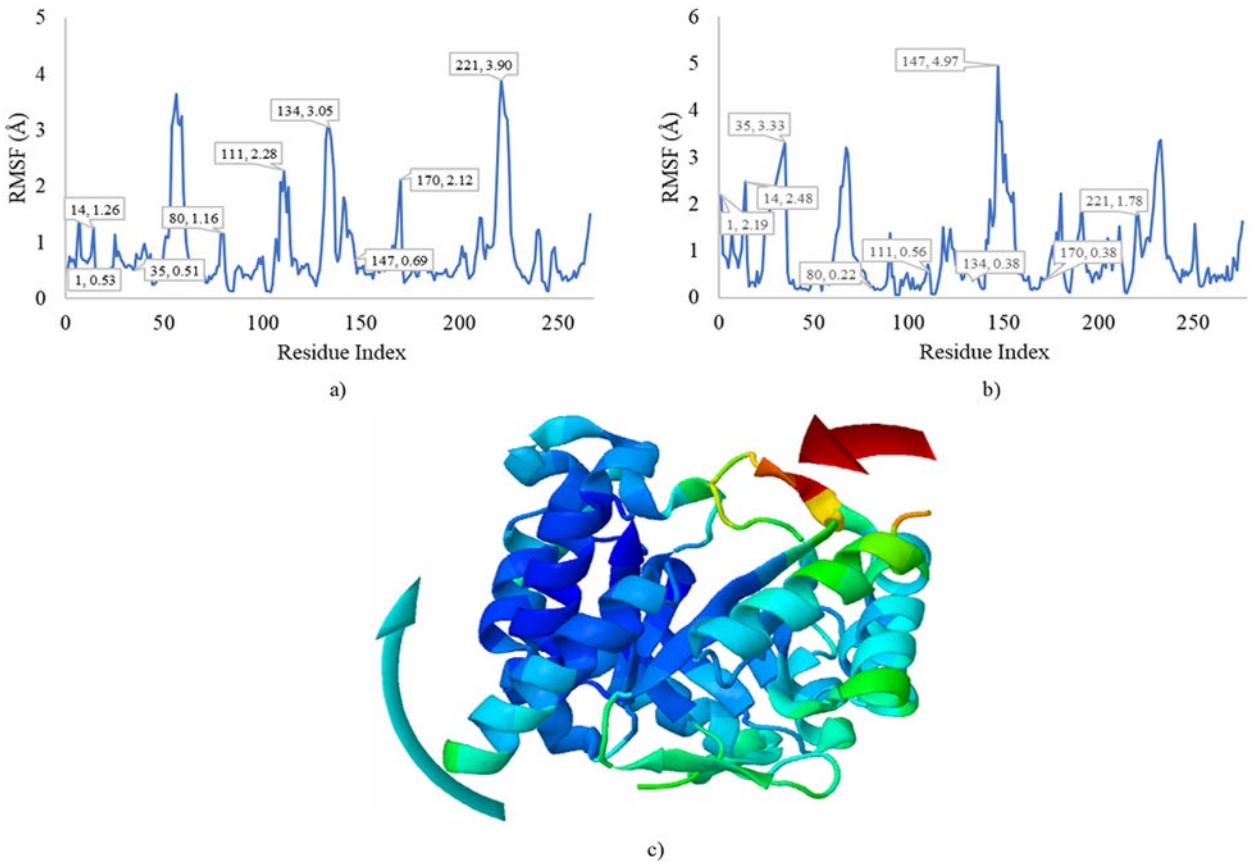

Figure 8: MDS result depicting residue fluctuation of; a) DHPS, b) Stigmasterol-DHPS docked complex, and c) Cluster displacement of the docked complex (blue and red arrows indicate higher and lower displacements respectively)

The docking interaction of MurA and TopoIV is presented in Table 5 revealing the BA and Ki. The most favorable docked pose with MurA was exhibited by stigmasterol demonstrating the least BA (-7.1 kcal/mol) and Ki (10.23 µM) followed by 4,4-dimethylcyclohex-2-en-1-ol with -6.8 kcal/mol and 10.23 µM respectively. Moreover, 5-acetoxymethyl-2-furaldehyde showed the highest BA (-5.1 kcal/mol) and Ki (180.94 µM). Stigmasterol also exhibited the least BA (-7.8 kcal/mol) and Ki (1.89 µM) interacting with TopoIV next to 4,4-dimethylcyclohex-2-en-1-ol with -5.7 kcal/mol and 65.65 µM respectively while 5-acetoxymethyl-2-furaldehyde had the highest -5.3 kcal/mol and 129.05 µM respectively.

The docking interaction of the stigmasterol-MurA docked complex is presented in a 2D and 3D docked pose in Figure 9. A single conventional hydrogen bond was observed with Lys90, while the alkyl bonds were observed with PHE330, ILE119, CYS117, and ARG93, all contributing to the stability of the complex.

Table 5: Binding affinity and Ki of the interaction of MurA and TopoIV with the compounds

Target	Ligand	Binding Affinity (kcal/mol)	Ki (µM)
MurA	Stigmasterol	-7.1	6.16
	4,4-Dimethylcyclohex-2-en-1-ol	-6.8	10.23
	5-Acetoxymethyl-2-furaldehyde	-5.1	180.94
TopoIV	Stigmasterol	-7.8	1.89
	4,4-Dimethylcyclohex-2-en-1-ol	-5.7	65.65
	5-Acetoxymethyl-2-furaldehyde	-5.3	129.05

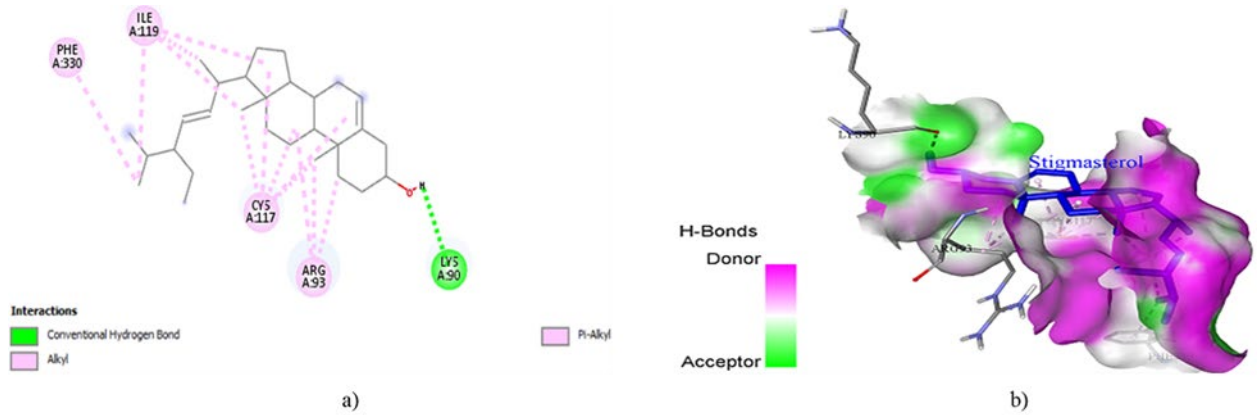

Figure 9: Dock poses and interactions of stigmasterol with MurA; a) 2D and b) 3D

The cluster displacement and residue fluctuation of MurA and stigmasterol-MurA docked complex observed from MDS are presented in Figure 10. All the residues fluctuated with the highest (3.38 Å) by THR69 though both terminals also fluctuated. Additionally, increased fluctuations were exhibited by GLU87 (1.84 Å) and LEU113 (2.51 Å) while CYS117 (1.90 Å), SER212 (1.93 Å), and HIS301 (1.41 Å) were decreased. Moreover, cluster displacement showed higher movement around the N-terminal than the C-terminal with the clusters moving in opposite directions.

Figure 11 depicts the 2D and 3D dock pose and binding interactions of the stigmasterol-TopoIV docked complex. A conventional hydrogen bond was formed between the ligand and ASP69, with additional alkyl interactions with residues MET74, ILE90, ALA86, LEU86, ARG93, and PRO75.

The cluster displacement and residue fluctuation of MDS of TopoIV and stigmasterol-TopoIV docked complex are presented in Figure 12. The highest (4.35 Å) fluctuation was exhibited by ALA61 (2.76 Å), though PRO196 (2.00 Å), ASN207 (2.21 Å), and TY215 (1.91 Å) exhibited increased displacements while GLY15 (2.85 Å), GLY73 (2.12 Å), and ASN207 (2.21 Å) were decreased. Moreover, a higher cluster displacement was observed from the N-terminal to the midchain with lower displacement at the C-terminal.

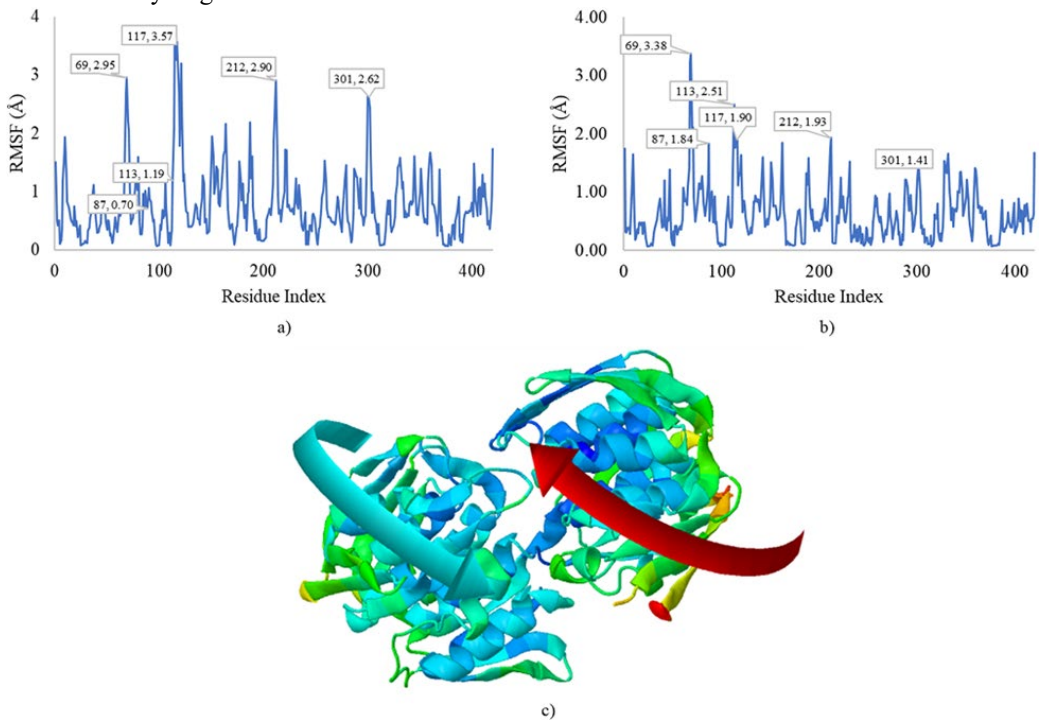

Figure 10: MDS result depicting residue fluctuation of; a) MurA, b) Stigmasterol-MurA docked complex, and c) Cluster displacement of the docked complex (blue and red arrows indicate higher and lower displacements respectively)

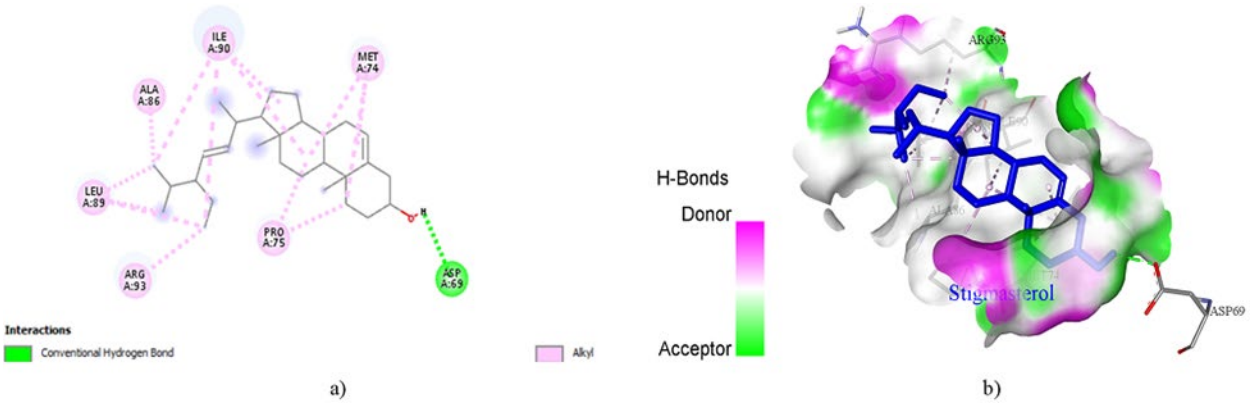

Figure 11: Dock poses and interactions of stigmasterol with TopoIV; a) 2D and b) 3D

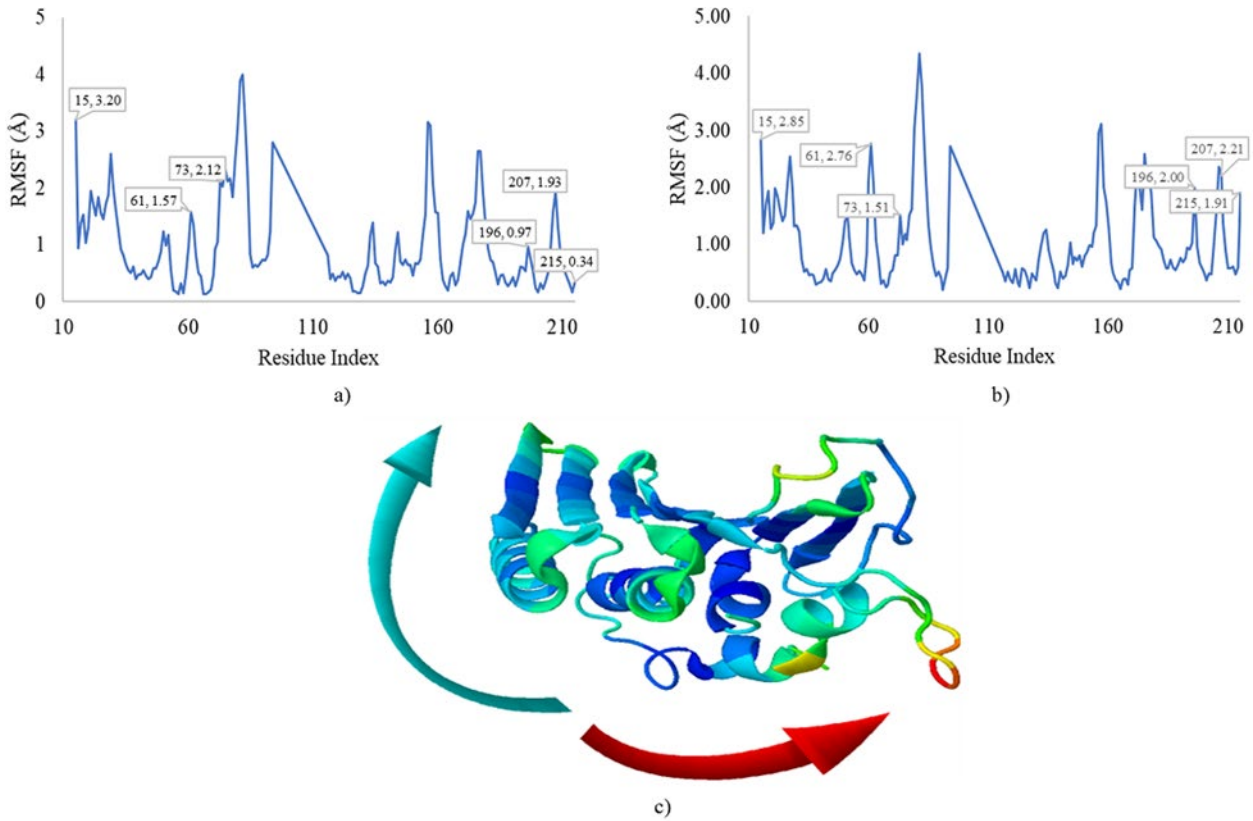

Figure 12: MDS result depicting residue fluctuation of; a) TopoIV, b) Stigmasterol-TopoIV docked complex, and c) Cluster displacement of the docked complex (blue and red arrows indicate higher and lower displacements respectively)

The ADMET prediction results of stigmasterol and 4,4-dimethylcyclohex-2-en-1-ol are shown in Table 6. Stigmasterol was predicted to be poorly soluble with low gastrointestinal absorption in addition to being a non-substrate but a P-glycoprotein inhibitor. Moreover, it has lipophilicity, water solubility, and skin permeation values of 6.98 Log $P_{o/w}$, -1.82 Log *S*, and -2.74 cm/s respectively. Predictively, stigmasterol have no blood-brain barrier permeability (BBB), fraction unbound (Fu) and volume of distribution (VD) and central nervous system (CNS) permeability of 0.176 log L/kg and -1.691 log PS respectively. Additionally, it's a CYP3A4 substrate and CYP2C9 inhibitor with a renal clearance of 0.618 log ml/min/kg and a non-renal organic cation transporter 2 (OCT2) substrate. Furthermore, stigmasterol is neither hepatotoxic, carcinogenic, mutagenic, nor, cytotoxic with 2.35 mol/kg LD50 and low toxicity (class 4).

For 4,4-dimethylcyclohex-2-en-1-ol, it is a moderately soluble compound with high gastrointestinal absorption and neither substrate nor inhibitor of the glycoproteins though it has lipophilicity, water solubility, and skin sensation of 3.90 Log $P_{o/w}$, -4.47 Log *S*, and -4.81 cm/s respectively. Furthermore, it is BBB permeant with VD, Fu, and CNS permeability of 0.553 L/kg, 0.177, and -2.23 log PS, respectively. However, it is a CYP2D6, CYP3A4, and renal OCT2 substrate and CYP2D6 inhibitor with a total clearance of 0.061 log ml/min/kg. Moreover, it is neither hepatotoxic, carcinogenic, mutagenic, nor cytotoxic but skin sensible with LD50 of 2.11 mol/kg.

Table 6: ADMET predictions of stigmasterol and 4,4-Dimethylcyclohex-2-en-1-ol

Parameters		Stigmasterol	4,4-Dimethylcyclohex-2-en-1-ol
Absorption	Lipophilicity (consensus Log $P_{o/w}$)	6.98	3.90
	Water solubility (consensus Log *S*)	-1.82	-4.47
	Solubility class	Poorly soluble	Moderately soluble
	GI absorption	Low	High
	Skin permeation [Log K_p (cm/s)]	-2.74	-4.81
	P-glycoprotein substrate	No	No
	P-glycoprotein I inhibitor	Yes	No
	P-glycoprotein II inhibitor	Yes	No
Distribution	The volume of distribution (log L/kg)	0.176	0.553
	Fraction unbound	0	0.177
	BBB permeability	No	Yes
	CNS permeability (log PS)	-1.691	-2.23
Metabolism	CYP1A2 inhibitor	No	No
	CYP2D6 substrate	No	Yes
	CYP3A4 substrate	Yes	Yes
	CYP2C19 inhibitor	No	No
	CYP2C9 inhibitor	Yes	No
	CYP2D6 inhibitor	No	Yes
	CYP3A4 inhibitor	No	No
Excretion	Total clearance (log ml/min/kg)	0.618	0.061
	Renal OCT2 substrate	No	No
Toxicity	LD50 (mol/kg)	2.35	2.11
	Toxicity Class	4	4
	Hepatotoxicity	No	No
	Skin Sensitisation	No	Yes
	Carcinogenicity	No	No
	Mutagenicity	No	No
	Cytotoxicity	No	No

The oral bioavailability radar of stigmasterol and 4,4-dimethylcyclohex-2-en-1-ol is presented in Figure 13 depicting its drug-like properties. Although the size, flexibility (FLEX), insaturation (INSATU), and polarity (POLAR) are within the accepted range, lipophilicity (LIPO) and insolubility (INSOLU) were out of range. However, the oral bioavailability radar of 4,4-dimethylcyclohex-2-en-1-ol falls within the acceptable pink range as shown in Figure 13.

The drug-likeness and medicinal chemistry of stigmasterol and 4,4-Dimethylcyclohex-2-en-1-ol are presented in Table 7. A bioavailability score of 0.55 was predicted for stigmasterol with single violations of Lipinski's and Verber rules though without any Egan violation. Although no PAINS alert was predicted, there were two lead-likeness violations with a synthetic accessibility of 6.21. For 4,4-dimethylcyclohex-2-en-1-ol, it has the same bioavailability score (0.55) as stigmasterol with neither violation of Lipinski's rule, Egan rule, nor Veber's rule, and PAINS alert, however, one lead likeness violation and 2.93 synthetic accessibility were observed.

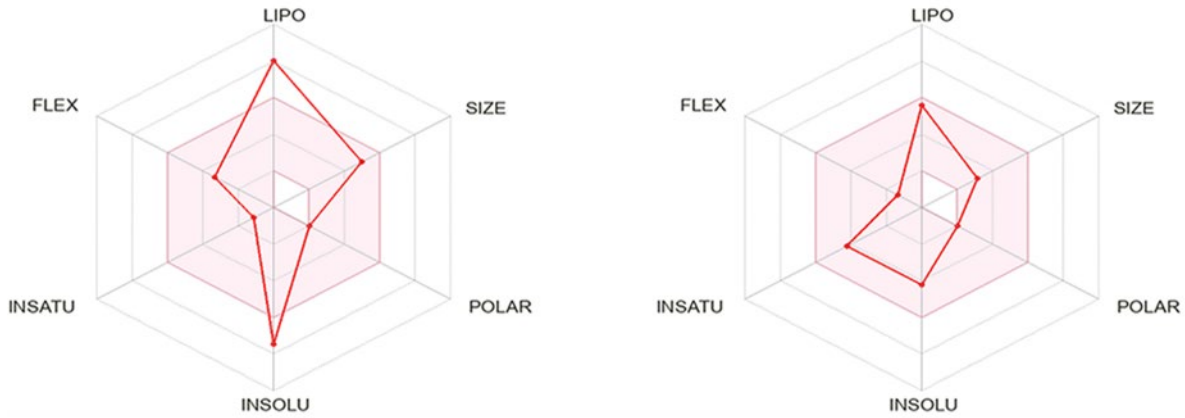

Figure 13: Oral bioavailability radars showing the LIPO (lipophilicity), flexibility (FLEX), insaturation (INSATU), and insolubility (INSOLU) of; A) Stigmasterol and B) 4,4-Dimethylcyclohex-2-en-1-ol

Table 7. Drug-likeness and medicinal chemistry of compounds stigmasterol and 4,4-Dimethylcyclohex-2-en-1-ol

Parameters		Stigmasterol	4,4-Dimethylcyclohex-2-en-1-ol
Druglikeness	Lipinski	Yes; 1 violation: MLOGP>4.15	Yes; 0 violation
	Egan	Yes	Yes
	Veber	No; 1 violation: WLOGP>5.88	Yes
	Bioavailability score	0.55	0.55
Medicinal chemistry	PAINS	0 alert	0 alert
	Lead likeness	No; 2 violations: MW>350, XLOGP3>3.5	No; 1 violation: XLOGP3>3.5
	Synthetic accessibility	6.21	2.93

Discussion

In the present study, the binding energy and interaction of identified compounds in XA with antimicrobial targets were investigated to determine the inhibitory potential of the compounds. The targets were selected due to their roles in the survival of bacterial cells *via* replication and metabolism of important metabolites. The FabI enzyme catalyzes the elongation step during fatty acid synthesis requiring NADH and NADPH as cofactors and, thus, a target for antibacterial therapeutics (Hopf et al., 2022). Stigmasterol interaction with FabI with low BA and Ki in the present study might demonstrate inhibition of the enzyme due to high affinity for the ligand, further revealed by the MDS with the several residue displacements within the protein structure. The last stage of bacterial cell wall synthesis (peptidoglycan) is catalyzed by PBP2X vital for the maintenance of cellular integrity, growth, and survival (Schweizer et al., 2014). PBP2X is a target of the antibacterial class of drugs β-lactams though resistance to drugs is possible by the lactamase enzymes produced by bacteria, which inactivate the enzymes (Peters et al., 2021). In our study, stigmasterol showed the most favorable docking with PBP2X with least BA and Ki, furthermore, the MDS showed several residue fluctuations, a possible inhibition of enzyme activity by stigmasterol.

DHFR is crucial to bacterial replication and survival due to its role in folate synthesis (Cao et al., 2018). It catalyzes the synthesis of (6s)-5,6,7,8-tetrahydrofolate (essential enzyme for DNA synthesis) from 7,8-dihydrofolate by reduction requiring NADH for the hydride transfer (Askari & Krajinovic, 2010; Cao et al., 2018). This enzyme is thus, a target of antibacterial drugs due to its absence in humans. Stigmasterol showed a favorable docked pose within the binding pocket of the enzyme with a low BA and Ki, possibly disrupting its activity due to its high affinity for the ligand. This is further supported by the MDS result which revealed fluctuations of the residues and cluster displacement depicting the flexibility of the formed complex. DHPS is another crucial enzyme required for the folate required for DNA synthesis, thus, an antibacterial drug target for the sulfonamides (Griffith et al., 2018). Specifically, it catalyzes the synthesis of 7,8-dihydropteroate (the substrate for DHFR) from 6-hydroxymethyl-7,8-dihydropteridine pyrophosphate and para-aminobenzoic acid (PABA) *via* condensation (Satuluri et al., 2020). In our study, stigmasterol also exhibited inhibitory potential against DHFR revealed by the docking interactions and low BA and Ki demonstrated by the docked complex. Furthermore, the MDS of the docked complex showed flexibility depicted by the hinge regions due to residue displacements.

MurA is a vital enzyme of peptidoglycan synthesis catalyzing the first committed step, the enolpyruvate group transfer from phosphoenolpyruvate to UDP-N-acetylglucosamine yielding UDP-N-acetylglucosamine enolpyruvate (de Oliveira et al., 2022; Hrast et al., 2014). Thus, an antibacterial target by its inhibitors like fosfomycin, covalently binding and inactivating the enzyme (de Oliveira et al., 2022). Stigmasterol also exhibited stable docking interaction with this enzyme with low BA and Ki possibly inhibiting its activity attributed to the high affinity for the ligand. Additionally, the MDS result showed several hinges regions depicting flexibility within the enzyme structure and cluster displacement at both peptide terminals, a possible disruption of its tertiary structure and activity. TopoIV is another vital bacterial enzyme involved in DNA synthesis during template separation and subsequent segregation of the daughter chromosomes (Helgesen et al., 2021). Therefore, it is a target for the antibacterial drugs fluoroquinolones, which decrease the rate of DNA synthesis and replication, generating double breaks leading to cell death (Hooper & Jacoby, 2016). Stigmasterol also showed promising antibacterial potential *via* inhibition of this enzyme due to the higher affinity of the enzyme for the ligand evidenced by the low BA and Ki interaction. Moreover, the MDS result also supports its potential due to the cluster movement and residue fluctuations.

We further investigated the pharmacological properties of stigmasterol and 4,4-dimethylcyclohex-2-en-1-ol for their ADMET drug-likeness and medicinal chemistry. 4,4-dimethylcyclohex-2-en-1-ol exhibited superior absorption properties with higher solubility and gastrointestinal absorption than stigmasterol, though both are not P-glycoprotein substrates. The P-glycoprotein acts as a barrier detoxifying the cell by extruding toxins and foreign compounds from the cell (Pires et al., 2015). Moreover, both compounds are skin permeable as a compound with skin permeability >-2.5 cm/h is considered permeable (Pires et al., 2015). Moreover, a steady-state volume of distribution (VDss) <-0.15 and >0.45 are regarded as low and high respectively (Pires et al., 2015). The compound with CNS >-2 is regarded as CNS penetrant. Stigmasterol has a moderate VDss while 4,4-Dimethylcyclohex-2-en-1-ol has higher VDss with the former being BBB permeable while the former has higher CNS permeability (Pires et al., 2015). Although both compounds are of the same toxicity class, 4,4-dimethylcyclohex-2-en-1-ol has skin sensation with lower LD50. Furthermore, the oral bioavailability showed 4,4-Dimethylcyclohex-2-en-1-ol demonstrate better drug-

likeness than stigmasterol without violations of the Lipinski's, Verber's, or Egan rule though both compounds are without PAINS alerts and lead-likeness. Summarily, 4,4-dimethylcyclohex-2-en-1-ol exhibited better pharmacological properties than stigmasterol.

Conclusion

In the present study, the antibacterial potential of the compounds identified in XA from our previous study was explored *via* molecular docking and molecular dynamics study. Furthermore, we explored the possibility of applying the top-docked compound as an antibacterial drug *via* its ADMET, lead-likeness, and medicinal properties. Stigmasterol exhibited the most favorable interaction with all the tested targets demonstrating the least BA and Ki among the compounds. In terms of drug-likeness, 4,4-dimethylcyclohex-2-en-1-ol showed good antibacterial potential with better drug and lead likeness than stigmasterol. Although stigmasterol has inferior drug and lead likeness properties, it exhibited better binding properties with all the enzymes, thus, structural modification might improve its weakness. Conclusively, stigmasterol and 4,4-dimethylcyclohex-2-en-1-ol might be responsible for the antibacterial effect of XA.

Authors Contributions

Conceptualization, D.M.M., A.M.A., and I.Y.; methodology, D.M.M.; investigation, D.M.M.; resources, A.M.A., and I.Y.X; writing-original draft preparation, D.M.M.; writing-review and editing, D.M.M. All authors have read and agreed to the published version of the manuscript.

Acknowledgement

The authors express their immense gratitude to the Pharmaceutical Technology Department, Adamawa State Polytechnic, Yola for institutional support.

Conflict of Interest

The authors declare no conflicts of interest.

References

Agustina, F., & Nugroho, R. P. P. (2021). Antibacterial Potential of Bidara Laut (Ximenia americana) Plant Against Vibrio alginolyticus and V. parahaemolyticus Bacteria. *Bioeduscience*, *5*(1), 15-23.

Askari, S. B., & Krajinovic, M. (2010). Dihydrofolate reductase gene variations in susceptibility to disease and treatment outcomes. *Current genomics*, *11*(8), 578-583.

Bakrim, W. B., Nurcahyanti, A. D. R., Dmirieh, M., Mahdi, I., Elgamal, A. M., El Raey, M. A., Wink, M., & Sobeh, M. (2022). Phytochemical profiling of the leaf extract of Ximenia americana var. Caffra and its antioxidant, antibacterial, and antiaging activities in vitro and in Caenorhabditis elegans: a cosmeceutical and dermatological approach. *Oxidative Medicine and Cellular Longevity*, *2022*, 3486257.

Cao, H., Gao, M., Zhou, H., & Skolnick, J. (2018). The crystal structure of a tetrahydrofolate-bound dihydrofolate reductase reveals the origin of slow product release. *Communications Biology*, *1*(1), 226. https://doi.org/10.1038/s42003-018-0236-y

Chassagne, F., Samarakoon, T., Porras, G., Lyles, J. T., Dettweiler, M., Marquez, L., Salam, A. M., Shabih, S., Farrokhi, D. R., & Quave, C. L. (2021). A Systematic Review of Plants With Antibacterial Activities: A Taxonomic and Phylogenetic Perspective [Systematic Review]. *Frontiers in Pharmacology*, *11*, 2020. https://www.frontiersin.org/articles/10.3389/fphar.2020.586548

Clegg, L. E., & Mac Gabhann, F. (2015). Molecular mechanism matters: Benefits of mechanistic computational models for drug development. *Pharmacological Research*, *99*, 149-154. https://doi.org/https://doi.org/10.1016/j.phrs.2015.06.002

Dahiru, M. M., Abaka, A. M., & Artimas, S. P. (2023a). Phytochemical Analysis and Antibacterial Activity of Methanol and Ethyl Acetate Extracts of Detarium microcarpum Guill. & Perr. Biology, Medicine, & Natural Product Chemistry, 12(1), 281-288.

Dahiru, M. M., Abaka, A. M., & Musa, N. (2023b). Phytochemical Analysis, In-vitro, and In-silico Antibacterial Activity of Stembark Extract of Anogeissus leiocarpus (DC) Guill and Perr. *Sciences of Pharmacy*, *2*(3), 24-41.

Dahiru, M. M., Badgal, E. B., & Musa, N. (2022). Phytochemistry, GS-MS analysis, and heavy metals composition of aqueous and ethanol stem bark extracts of Ximenia americana. *GSC Biological and Pharmaceutical Sciences*, *21*(3), 145-156.

Daina, A., Michielin, O., & Zoete, V. (2017). SwissADME: a free web tool to evaluate pharmacokinetics, drug-likeness and medicinal chemistry friendliness of small molecules. *Scientific Reports*, *7*(1), 42717.

de Menezes, I. R. A., da Costa, R. H. S., Augusti Boligon, A., Rolón, M., Coronel, C., Vega, C., Melo Coutinho, H. D., da Costa, M. S., Tintino, S. R., Silva Pereira, R. L., de Albuquerque, T. R., da Silva Almeida, J. R. G., & Quintans-Júnior, L. J. (2019). Ximenia americana L. enhances the antibiotic activity and inhibit the development of kinetoplastid parasites. *Comparative Immunology, Microbiology and Infectious Diseases*, *64*, 40-46. https://doi.org/https://doi.org/10.1016/j.cimid.2019.02.007

de Oliveira, M. V. D., Furtado, R. M., da Costa, K. S., Vakal, S., & Lima, A. H. (2022). Advances in UDP-N-Acetylglucosamine Enolpyruvyl Transferase (MurA) Covalent Inhibition [Mini Review]. *Frontiers in Molecular Biosciences*, *9*, 889825. https://www.frontiersin.org/articles/10.3389/fmolb.2022.889825

Doughari, J. H. (2012). *Phytochemicals: extraction methods, basic structures and mode of action as potential chemotherapeutic agents*. INTECH Open Access Publisher Rijeka, Croatia.

Ebbo, A. A., Sani, D., Suleiman, M. M., Ahmed, A., & Hassan, A. Z. (2019). Phytochemical Composition, Proximate Analysis and Antimicrobial Screening of the Methanolic Extract of Diospyros mespiliformis Hochst Ex a. Dc (Ebenaceae). *Pharmacognosy Journal*, *11*(2), 362-368.

Gajdács, M., & Albericio, F. (2019). Antibiotic resistance: from the bench to patients. *Antibiotics*, *8*(3), 129.

Griffith, E. C., Wallace, M. J., Wu, Y., Kumar, G., Gajewski, S., Jackson, P., Phelps, G. A., Zheng, Z., Rock, C. O., Lee, R. E., & White, S. W. (2018). The Structural and Functional Basis for Recurring Sulfa Drug Resistance Mutations in Staphylococcus aureus Dihydropteroate Synthase [Original Research]. *Frontiers in Microbiology*, *9*, 1369. https://www.frontiersin.org/articles/10.3389/fmicb.2018.01369

Helgesen, E., Sætre, F., & Skarstad, K. (2021). Topoisomerase IV tracks behind the replication fork and the SeqA complex during DNA replication in Escherichia coli. *Scientific Reports*, *11*(1), 474. https://doi.org/10.1038/s41598-020-80043-4

Hollingsworth, S. A., & Dror, R. O. (2018). Molecular dynamics simulation for all. *Neuron*, *99*(6), 1129-1143.

Hooper, D. C., & Jacoby, G. A. (2016). Topoisomerase inhibitors: fluoroquinolone mechanisms of action and resistance. *Cold Spring Harbor Perspectives in Medicine*, *6*(9), a025320.

Hopf, F. S. M., Roth, C. D., de Souza, E. V., Galina, L., Czeczot, A. M., Machado, P., Basso, L. A., & Bizarro, C. V. (2022). Bacterial Enoyl-Reductases: The Ever-Growing List of Fabs, Their Mechanisms and Inhibition [Review]. *Frontiers in Microbiology*, *13*, 2020. https://www.frontiersin.org/articles/10.3389/fmicb.2022.891610

Hrast, M., Sosič, I., Šink, R., & Gobec, S. (2014). Inhibitors of the peptidoglycan biosynthesis enzymes MurA-F. *Bioorganic Chemistry*, *55*, 2-15. https://doi.org/https://doi.org/10.1016/j.bioorg.2014.03.008

Jendele, L., Krivák, R., Škoda, P., Novotný, M., & Hoksza, D. (2019). PrankWeb: a web server for ligand binding site prediction and visualization. *Nucleic Acids Research*, *47*, 345-349. https://doi.org/10.1093/nar/gkz424

Kapoor, G., Saigal, S., & Elongavan, A. (2017). Action and resistance mechanisms of antibiotics: A guide for clinicians. *Journal of Anaesthesiology, Clinical Pharmacology*, *33*(3), 300–305.

Kiessoun, K., Roland, M. N. T., Mamounata, D., Yomalan, K., Sytar, O., Souz, A., Brestic, M., & Dicko, M. H. (2018). Antimicrobial profiles, antidiarrheal and antipyretic capacities of phenol acid rich-fractions from Ximenia america L.,(Olacaceae) in wistar albino rats. *Int J Pharm Pharm Sci*, *10*, 62-70.

Kurcinski, M., Oleniecki, T., Ciemny, M. P., Kuriata, A., Kolinski, A., & Kmiecik, S. (2019). CABS-flex standalone: a simulation environment for fast modeling of protein flexibility. *Bioinformatics*, *35*(4), 694-695.

Lin, X., Li, X., & Lin, X. (2020). A review on applications of computational methods in drug screening and design. *Molecules*, *25*(6), 1375.

López-Blanco, J. R., Aliaga, J. I., Quintana-Ortí, E. S., & Chacón, P. (2014). iMODS: internal coordinates normal mode analysis server. *Nucleic Acids Research*, *42*(W1), W271-W276.

MacGowan, A., & Macnaughton, E. (2017). Antibiotic resistance. *Medicine*, *45*(10), 622-628.

Maikai, V., Maikai, B. V., & Kobo, P. (2009). Antimicrobial Properties of Stem Bark Extracts of Ximenia Americana. *Journal of Agricultural Science*, *1*, 30-34. https://doi.org/10.5539/jas.v1n2p30

Monte, F. J. Q., de Lemos, T. L. G., de Araújo, M. R. S., & de Sousa Gomes, E. (2012). Ximenia americana: chemistry, pharmacology and biological properties, a review. *Phytochemicals–A Global Perspective of Their Role in Nutrition and Health*, 429-450.

Ortiz, C. L. D., Completo, G. C., Nacario, R. C., & Nellas, R. B. (2019). Potential Inhibitors of Galactofuranosyltransferase 2 (GlfT2): Molecular Docking, 3D-QSAR, and In Silico ADMETox Studies. *Scientific Reports*, *9*(1), 17096. https://doi.org/10.1038/s41598-019-52764-8

Peters, K., Schweizer, I., Hakenbeck, R., & Denapaite, D. (2021). New Insights into Beta-Lactam Resistance of Streptococcus pneumoniae: Serine Protease HtrA Degrades Altered Penicillin-Binding Protein 2x. *Microorganisms*, *9*(8).

Pires, D. E. V., Blundell, T. L., & Ascher, D. B. (2015). pkCSM: Predicting Small-Molecule Pharmacokinetic and Toxicity Properties Using Graph-Based Signatures. *Journal of Medicinal Chemistry*, *58*(9), 4066-4072. https://doi.org/10.1021/acs.jmedchem.5b00104

Raval, K., & Ganatra, T. (2022). Basics, types and applications of molecular docking: A review. *IP International Journal of Comprehensive and Advanced Pharmacology*, *7*(1), 12-16.

Sanner, M. F. (1999). Python: a programming language for software integration and development. *Journal of Molecular Graphics and Modelling*, *17*(1), 57-61.

Satuluri, S. H., Katari, S. K., Pasala, C., & Amineni, U. (2020). Novel and potent inhibitors for dihydropteroate synthase of Helicobacter pylori. *Journal of Receptors and Signal Transduction*, *40*(3), 246-256. https://doi.org/10.1080/10799893.2020.1731533

Schweizer, I., Peters, K., Stahlmann, C., Hakenbeck, R., & Denapaite, D. (2014). Penicillin-binding protein 2x of Streptococcus pneumoniae: the mutation Ala707Asp within the C-terminal PASTA2 domain leads to destabilization. *Microbial Drug Resistance*, *20*(3), 250-257.

Sliwoski, G., Kothiwale, S., Meiler, J., & Lowe, E. W. (2014). Computational methods in drug discovery. *Pharmacological Reviews*, *66*(1), 334-395.

Uddin, T. M., Chakraborty, A. J., Khusro, A., Zidan, B. M. R. M., Mitra, S., Emran, T. B., Dhama, K., Ripon, M. K. H., Gajdács, M., Sahibzada, M. U. K., Hossain, M. J., & Koirala, N. (2021). Antibiotic resistance in microbes: History, mechanisms, therapeutic strategies and future prospects. *Journal of Infection and Public Health*, *14*(12), 1750-1766. https://doi.org/https://doi.org/10.1016/j.jiph.2021.10.020

Zaman, S. B., Hussain, M. A., Nye, R., Mehta, V., Mamun, K. T., & Hossain, N. (2017). A Review on Antibiotic Resistance: Alarm Bells are Ringing. *Cureus*, *9*(6), e1403. https://doi.org/10.7759/cureus.1403